Real-Time Validation of a Sliding Mode Controller for Closed-Loop Operation of Reduced Switch Count Multilevel Inverters

G. Eshwar Gowd , P. C. Sekhar, *Member, IEEE*, and Dharmavarapu Sreenivasarao

Abstract—The prominence of reduced switch count multilevel inverters is rising owing their merits of decreased number of switches and modular structures. There are topologies that use more than one source; however, utilization of all the sources at all levels is seldom. These topologies will diminish the energy efficiency of the conversion system as all the sources will not deliver the power except at the highest level in the output voltage. These kinds of converters can hamper the penetration of renewable energy into the existing energy mix, as the energy capacity of the renewable source is undermined. In this connection, this paper explores a three-phase multilevel inverter that can extract the power from all the sources at all the levels through series/parallel switchings. Besides, this paper develops a sliding mode based nonlinear controller for closed-loop operation of the multilevel inverter, which is not addressed sufficiently in the literature. The performance of the developed variable gain nonlinear controller is validated against the PI controller for delivering desired powers under different operating conditions/disturbances using simulations and in real-time environment.

Index Terms—Closed-loop control, multilevel inverters (MLIs), nonlinear control, real-time validations, reduced switch count (RSC) topologies, sliding mode control (SMC), source utilization.

NOMENCLATURE

v_{dg}, v_{qg}	Grid voltages at PCC in the d–q frame of reference.
i_{dg}, i_{qg}	Grid currents at PCC in the d–q frame of reference.
$v_{d\text{inv}}, v_{q\text{inv}}$	Multilevel inverter voltages in the d–q frame of reference.
ω	Angular frequency of grid voltage.
σ	Sliding surface.
q_n	Relative degree of an output state variable.
λ	State vector matrix.
Y	Output states matrix.
G	Lyapunov function.
UF	Utilization factor of input dc sources of a multilevel inverter.

I. INTRODUCTION

FOR feeding the power from a distributed source to the grid, the common practice is to employ two-level inverters. However, injecting high powers into the grid using two-level inverters necessitates higher dc voltages with increased power levels. Since the inverter has to handle high voltage and powers, the switches should also be able to withstand the high voltages and their rate of changes. On the other hand, the two-level inverters will be having large filtering requirements at high power handling capacities. Hence, for the high power grid feeding applications from distributed sources, a multilevel inverter (MLI) is an attractive choice against the two-level inverters. The focus on MLIs is increasing because of their ability in improving the quality of the output voltage, reducing the total harmonic distortion (THD), and low *dv/dt* in the output. In addition, the MLIs can be realized with switches of low ratings. Cascaded H-bridge (CHB), diode clamped, and flying capacitor are different conventional MLI topologies. However, in recent days, there is a transition of focus from conventional MLIs to reduced switch count (RSC) topologies, as in [1]–[6]. As it is there in its name, the RSC topologies can contribute to higher number of levels with less number of circuit devices, lower number of ON state switches, and they involve modular structures [7]–[9]. For example, the prime objective of [7] is to maximize the number of voltage levels by using reduced number of dc voltage sources and reduced number of components per required pole voltage levels, whereas the idea of [9] is to realize the MLI with less number of switches. Even though all the existing MLI configurations are capable of delivering output with the aforesaid advantages, the utilization of dc sources is poor. This is due to disconnection of dc sources from the load at most of the voltage levels in these configurations. Even though the configurations developed in [10] and [11] show good performance in utilizing input dc sources at all the levels, they have only one input dc source and more number of capacitors. The limitation of these configurations is that the number of capacitors increases with number of levels. Moreover, the charging and discharging cycles of the capacitors have to be carefully managed for stable and satisfactory operation of the converter. In addition, as these configurations [10], [11] consist of only one voltage source and the MLIs are put in service to produce high voltage and high power levels, it necessitates a source of high power ratings. The limitations of [10] and [11] can be overcome by employing CHB-based topology [12]. However, in

conventional CHB topologies, all the dc sources will be in use only at a peak voltage level. To address the shortcomings of switched capacitor and CHB configurations, a topology is proposed in [13]; however, it is for single-phase applications. The configuration proposed in [13] is an RSC topology and consists of more than one source (number of sources will depend on number of required levels, as explained later in this paper). Different voltage levels are achieved through series/parallel switching of sources. This specific merit of switched series/parallel sources (SSPS) of [13] is found to be advantageous for various grid-connected applications, as it helps in better utilization of photovoltaic (PV) and other renewable energy based sources so that increased power outputs can be achieved. This feature of SSPS is also important as it ensures uniform utilization of dc sources; hence, the aging of sources will be more or less uniform. Hence, SSPS topology calls for less maintenance and replacement costs when compared with CHB topologies as their nonuniform utilization demands frequent replacement of one or other sources. Given its advantages, the topology proposed in [13] is considered for the analysis in this paper and has been adopted for three-phase systems as RSC-based MLI with SSPS (RSC-SSPS). Even though a good number of MLI topologies are evolved, the closed-loop control of the MLI, the critical task in integrated operation of the MLI with grid/load, has not been sufficiently addressed in the literature, excluding very few [14]–[18].

In order to obtain satisfactory power transfer, which is indeed dependent on pulsewidth modulation (PWM) switching control, the required reference signal can be obtained by a conventional PI controller as in [14]–[16]. The employed PI controllers in [14] and [16] are linear controllers and their number increases with increase in number of sources; hence, their tuning is a challenging task to achieve satisfactory operation. Two other control schemes, namely, plug-in repetitive control and model predictive control are employed in [17] and [18] for reducing the circulating currents and balancing capacitor voltages in a modular multilevel converter system, respectively. Even though the controllers in [14]–[18] achieved closed-loop control, they used either linear controllers or the system operation is limited to islanding operation with linear controllers. None of them have explored the closed-loop control of the MLI with a nonlinear controller for feeding set point powers to the grid. The MLI-based grid-connected distributed generation (DG) system is a highly nonlinear system as it involves more switching actions and the circuit seen from the grid side will be different at different output voltage levels. Since the structure of the converter is changing at every level, it is a cumbersome process to tune the PI controllers to achieve successful, decoupled, and set point real and reactive powers in grid-connected MLIs. Moreover, the PI controller performance degrades if the operating point and/or the disturbance is different from that for which the controllers have been tuned. In addition, the PI controllers do not have disturbance rejection property as well as their performance is prone to parameter changes and prevailing model oscillations. To alleviate the shortcomings of the PI controller, the nonlinear system has to be linearized and a suitable control philosophy has to be developed. One of such approaches is sliding mode con-

trol (SMC) [19], [20]. SMC is suitable for linear and nonlinear systems and offers good robustness for systems like grid-connected MLIs. It slides over the surface as defined and is asymptotically stable. The switching is independent of system operating points and other circuit parameters. One of such controller is adopted in [21]; however, the MLI considered is a single source based one with relatively large number of switches. Hence, the aforementioned limitations of single source based MLIs with increased switch count will prevail in this case as well. Moreover, it has considered "sign" based control, a hard switching control, which can result in chattering performance, hence the introduction of unmodeled frequency components into the output. Even though the literature [14]–[21] considered the closed-loop control, it is limited either to conventional MLI topologies or two-level inverters. To the best of author's knowledge, the closed-loop control of RSC-based MLIs using nonlinear control for grid-connected operation to deliver set-point real and reactive powers is not explored in the literature.

In this connection, this paper developed a three-phase RSC-SSPS-based MLI with an objective to deliver set point real and reactive powers to the grid. The closed-loop control of the MLI has been achieved with help of soft switching function based SMC, which can deliver decoupled real and reactive power control with zero steady-state error. The robust performance of the controller is validated for different operating conditions and their changes, other grid parameter changes. The superiority of the control scheme is established against the conventional PI controller through different simulation case studies, which have been further validated in a real-time using Opal-RT test bed.

In addition to the aforementioned, this paper introduces a new performance indicator named "utilization factor" (UF) to quantify the utilization of dc sources. Even though the MLIs are well researched, the thrust is there in producing number of levels with minimum THD, switch stress, and loss minimization. However, the amount of utilization of the dc source in a full cycle of the output voltage is not explored to sufficient extent in the literature. Hence, this paper introduces UF and evaluates the same for different MLI topologies, which is helpful in selecting the MLI for a given application.

Rest of this paper is organized as follows. Section II describes the system configuration. The MLI topology and the utilization of the sources for different topologies are assessed in Section III. The conventional closed-loop control of the MLI and the linearization of the grid-connected MLI system are discussed in Section IV, while Section V discusses the integration of sliding mode concepts with the developed controller. Simulation results and their real-time validations are reported in Section VI. This paper is concluded in Section VII.

II. SYSTEM CONFIGURATION

Block diagram of the system considered with the RSC-SSPS MLI, feeding set point real and reactive powers (P_{ref} and Q_{ref}) to the three-phase grid, is shown in Fig. 1.

The closed-loop control of the RSC-SSPS MLI is achieved by employing either a PI controller or by developed SMC-based nonlinear controller. The controller, in turn, generates the

This article has been accepted for inclusion in a future issue of this journal. Content is final as presented, with the exception of pagination.

ESHWAR GOWD *et al.*: REAL-TIME VALIDATION OF A SLIDING MODE CONTROLLER FOR CLOSED-LOOP OPERATION OF REDUCED SWITCH 3
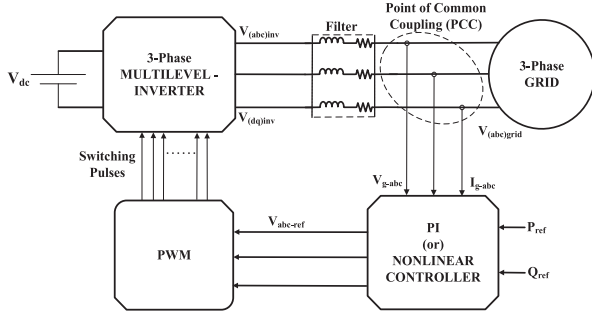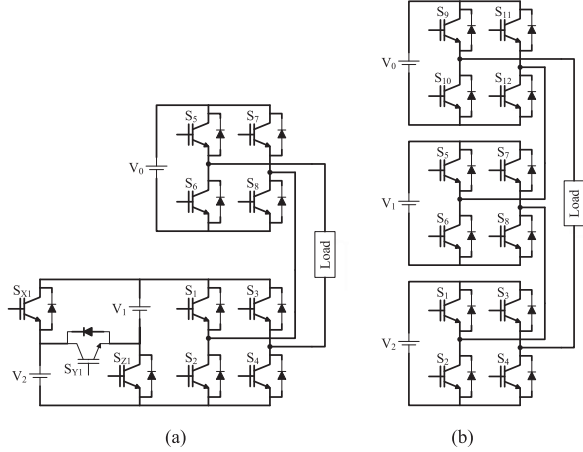
Fig. 1. Grid-connected MLI system layout.

Fig. 2. 11-level asymmetrical MLI topologies with 1:2 dc voltage ratios. (a) Asymmetrical SSPS RSC-MLI. (b) Asymmetrical CHB MLI.

modulating signal references, hence the switching pulses for the MLI, as shown in Fig. 1.

III. RSC-SSPS MLI TOPOLOGY

Among the various RSC-MLI topologies reported so far, SSPS is an efficient topology with self-balancing nature of dc voltages by series/parallel operation of capacitor or dc sources. In general, for any topology, voltage level is obtained by series-connected operation of capacitors or dc voltages sources. However, different voltage levels can be achieved through series/parallel-connected operation of the capacitors or dc voltages sources in SSPS topology, which increases the utilization of dc sources.

The considered RSC-SSPS MLI is shown in Fig. 2(a); the voltage sources of the upper and lower part of the SSPS MLI are considered as $V_0 = V$ and $V_1 = V_2 = 2 V$. When S_{Y1} is ON, V_1 and V_2 are in series, when S_{X1} and S_{Z1} are ON, V_1 and V_2 are in parallel. This operation will holds good for any "n" number of levels by increasing modules in the lower part of the converter. This MLI has been adopted from [13] and is developed for a three-phase system in this paper. For the detailed discussion on the working of the topology, readers may refer to [13].

A. Utilization Factor of Input DC Sources

To quantify the effective use of available dc sources in a full cycle of the output voltage of the MLI, a performance indicator

TABLE I
SWITCHING STATES AND THEIR CORRESPONDING DC SOURCES TO OBTAIN A PARTICULAR LEVEL IN PHASE VOLTAGE FOR 11-LEVEL ASYMMETRIC SSPS AND CHB MLIS WITH $V_0 = V$ AND $V_1 = V_2 = 2 V$

Phase voltage level	SSPS		CHB	
	Switching path	No. of Connected dc sources	Switching path	No. of Connected dc sources
+5V	S_{Y1}-S_1-S_8-S_5-S_4	V_1,V_2,V_0 (3)	S_1-S_8-S_5-S_{12}-S_9-S_4	V_1,V_2,V_0 (3)
+4V	S_{Y1}-S_1-S_7-S_5-S_4	V_1,V_2 (2)	S_1-S_8-S_5-S_{12}-S_{10}-S_4	V_1,V_2 (2)
+3V	S_{X1}-S_1-S_8-S_5-S_4-S_{Z1}	V_1,V_2,V_0 (3)	S_1-S_8-S_5-S_{11}-S_{10}-S_4	V_1,V_2,V_0 (3)
+2V	S_{X1}-S_1-S_7-S_5-S_4-S_{Z1}	V_1,V_2 (2)	S_1-S_8-S_6-S_{12}-S_{10}-S_4	V_2 (1)
+V	S_{X1}-S_1-S_7-S_6-S_4-S_{Z1}	V_1,V_2,V_0 (3)	S_1-S_8-S_5-S_{11}-S_{10}-S_3	V_1,V_0 (2)
0	S_2-S_8-S_6-S_4	0	S_1-S_8-S_6-S_{12}-S_{10}-S_3	0
−V	S_{Z1}-S_2-S_8-S_5-S_3-S_{X1}	V_1,V_2,V_0 (3)	S_1-S_7-S_6-S_{12}-S_9-S_3	V_1,V_0 (2)
−2V	S_{Z1}-S_2-S_8-S_6-S_3-S_{X1}	V_1,V_2 (2)	S_1-S_7-S_6-S_{11}-S_9-S_3	V_1 (1)
−3V	S_{Y1}-S_2-S_8-S_5-S_3	V_1,V_2,V_0 (3)	S_2-S_7-S_6-S_{12}-S_9-S_3	V_1,V_2,V_0 (3)
−4V	S_{Y1}-S_2-S_8-S_6-S_3	V_1,V_2 (2)	S_2-S_7-S_6-S_{12}-S_{10}-S_3	V_1,V_2 (2)
−5V	S_{Y1}-S_2-S_7-S_6-S_3	V_1,V_2,V_0 (3)	S_2-S_7-S_6-S_{11}-S_{10}-S_3	V_1,V_2,V_0 (3)

known as UF of input dc sources is introduced in this paper. Consider "N" is number of dc sources, "n" is the number of phase-voltage levels, and "X_j" is the number of dc sources connected in series/parallel to obtain the jth level in phase voltage, then the UF can be defined as

$$\text{UF} = \left. \begin{array}{c} \text{Sum of number of voltage sources connected to MLI} \\ \text{at each phase voltage level} \\ \hline \left(\begin{array}{c} \text{Total number of phase voltage levels} \\ \times \\ \text{Total number of sources in MLI} \end{array} \right) \end{array} \right\}.$$

$$\text{UF} = \frac{\sum_{j=1}^{n} X_j}{n \times N} \quad (1)$$

Consider an 11-level asymmetric CHB MLI and 11-level asymmetric SSPS RSC-MLI topologies, as shown in Fig. 2. Table I shows the switching states and their corresponding dc sources in connection to obtain a particular level in phase voltage for the topologies shown in Fig. 2.

In Table I, for example, number of dc sources connected to obtain a voltage level of $+V$ in the CHB MLI is 2, whereas in the SSPS-MLI, it is 3. Therefore, from Table I, the UFs for the asymmetrical topologies shown in Fig. 2 can be calculated as

$$\text{UF}_{\text{SSPS}} = (3+2+3+2+3+0+3+2+3+2+3)/$$
$$(11 \times 3) = 0.79$$

$$\text{UF}_{\text{CHB}} = (3+2+3+1+2+0+2+1+3+2+3)/$$
$$(11 \times 3) = 0.66.$$

The percentage increase in utilization of dc sources in the SSPS MLI with respect to the CHB MLI can be calculated as $[(\text{UF}_{\text{SSPS}} - \text{UF}_{\text{CHB}})/ \text{UF}_{\text{CHB}}] \times 100$. Therefore, from the above-mentioned calculations, it can be inferred that the utilization of dc voltage sources in SSPS topology is increased by 19.6% when compared with CHB topology. In case for 19 levels, the percentage increase in utilization of dc sources in SSPS topology is increased by 23.7% as compared to the same level CHB, as presented in Table II. This specific merit of SSPS is found to be advantageous for various grid-connected applications, as it helps in better utilization of PV and other renewable energy based

TABLE II
UTILIZATION FACTORS OF SSPS AND CHB FOR DIFFERENT
PHASE VOLTAGE LEVELS

Phase voltage levels	UF of SSPS	UF of CHB	% Increase in UF
11	0.79	0.66	19.6%
19	0.88	0.715	23.7%
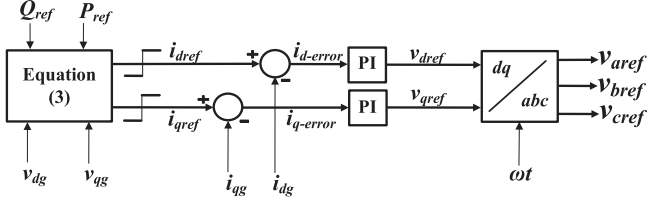
Fig. 3. Active and reactive power control using a conventional two-loop PI controller.

Fig. 4. Active and reactive power control using SMC.

sources. This feature of SSPS is also important as it ensures uniform utilization of dc sources; hence, the aging of sources will be more or less uniform. Therefore, SSPS topology calls for less maintenance and replacement costs when compared with CHB topologies as their nonuniform utilization will call for frequent replacement of one or other sources.

IV. CONVENTIONAL CLOSED-LOOP CONTROL STRATEGY FOR GRID-CONNECTED SSPS MLI AND LINEARIZATION

The main control objective in this MLI-based DG system is to supply the required amount of power(s) to the grid. This can be achieved by controlling the MLI with a conventional PI controller, in which the modulating voltages are derived by PI controllers, after directly processing the errors in the powers. However, due to the lack of inner current loop, this direct power control mechanism may result in current overshoots there by activating the protection circuitry of the switching converters. In some cases, these high converter currents can damage the switches and its associated devices. Hence, a two-loop-based power control mechanism is considered in this paper. However, in two-loop control, the reference currents are generated by PI controllers, which process the power errors. These current references are compared with actual currents to derive the errors in currents. These current errors are further processed in second set of PI controllers to generate the modulating voltages. Therefore, this methodology involves two sets of PI controllers to deliver desired real and reactive powers. The MLI-based grid-connected DG system is a highly nonlinear system with multiple switchings across different voltage sources within a single cycle to achieve multilevels in its output. With this highly nonlinear converter based DG system, the tuning of the PI controller is a challenging task. With two sets of PI controllers in the control loop, the tuning process becomes much more complex. Hence, to minimize the tuning complexity, a control mechanism with limited current references is developed, as shown in Fig. 3.

The real and reactive powers (P_g and Q_g) flowing in the system are given by (2). The current references (i_{dref} and i_{qref}) are estimated using (3). These estimated current references are in turn used to generate the modulating voltages, thereby
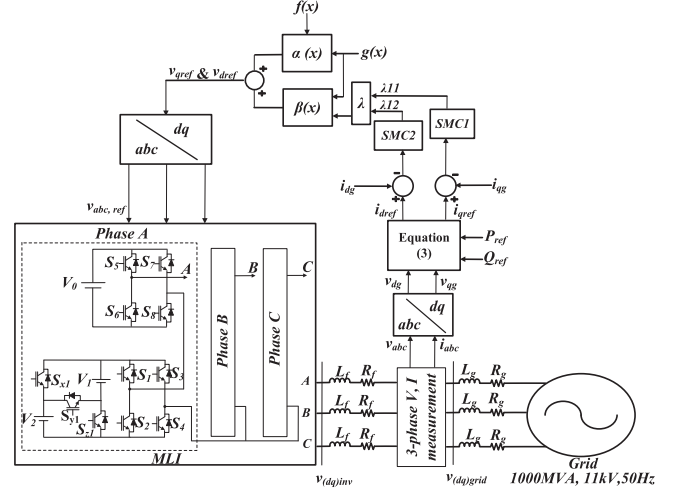
eliminating one set of PI controllers

$$P_g = (v_{dg}i_{dg}) + (v_{qg}i_{qg}) \text{ and } Q_g = (v_{qg}i_{dg}) - (v_{dg}i_{qg}) \quad (2)$$

$$i_{dref} = \frac{v_{qg}Q_{ref} + v_{dg}P_{ref}}{v_{dg}^2 + v_{qg}^2} \text{ and } i_{qref} = \frac{v_{qg}P_{ref} - v_{dg}Q_{ref}}{v_{dg}^2 + v_{qg}^2}. \quad (3)$$

Even though the modified two-loop PI control reduces the complexity, its capability in decoupling the real and reactive power controls is poor. It is due to the multivariable structure and highly coupled nonlinearity of the MLI-based grid-connected system. Moreover, the PI controller is sensitive to system parameter variations. Hence, it is necessary to transform the coupled and nonlinear system into decoupled and linear system by adopting a feedback linearization technique, which is explained as follows.

The interconnecting system shown in Fig. 4, from the output of the MLI up to the point of coupling with the grid, can be represented in a nonlinear dynamic mathematical model as

$$v_{dinv} - R_f i_{dg} - L_f \frac{di_{dg}}{dt} + \omega L_f i_{qg} - v_{dg} = 0 \quad (4)$$

$$v_{qinv} - R_f i_{qg} - L_f \frac{di_{qg}}{dt} - \omega L_f i_{dg} - v_{qg} = 0. \quad (5)$$

Consider the standard state-space representation as

$$\frac{dx}{dt} = f(x) + g(x)u. \quad (6)$$

The coupled and nonlinear system can be transformed into decoupled and linear system by rearranging (4) and (5), in the form of (6) with i_{dg} and i_{qg} as state variables, which results

$$f(x) = \begin{bmatrix} -\frac{R_f}{L_f}i_{dg} + \frac{X_f}{L_f}i_{qg} - \frac{1}{L_f}v_{dg} \\ -\frac{R_f}{L_f}i_{qg} - \frac{X_f}{L_f}i_{dg} - \frac{1}{L_f}v_{qg} \end{bmatrix}$$

$$g(x) = \begin{bmatrix} \frac{1}{L_f} & 0 \\ 0 & \frac{1}{L_f} \end{bmatrix} \quad x = \begin{bmatrix} i_d \\ i_q \end{bmatrix} \quad u = \begin{bmatrix} v_{dinv} \\ v_{qinv} \end{bmatrix}. \quad (7)$$

From (7), it can be said that there is a possible decoupling existing between the currents i_{dg} and i_{qg}.

After linearization, the system can also be represented as

$$\lambda = A(x) + B(x)U. \tag{8}$$

In order to obtain the control input to the MLI switching operation, the above-mentioned equation can be written as

$$U = (-B^{-1}(x) * A(x)) + (B^{-1}(x) * \lambda) \text{ or } U = \alpha(x) + \beta(x)\lambda \tag{9}$$

where $\alpha(x) = -B^{-1}(x) * A(x)$ and $\beta(x) = B^{-1}(x)$

$$B(x) = \begin{bmatrix} g_{11}(x) & 0 \\ 0 & g_{22}(x) \end{bmatrix} A(x) = \begin{bmatrix} f_{11}(x) \\ f_{21}(x) \end{bmatrix} \tag{10}$$

$$\lambda = [\lambda_{11} \ \lambda_{12}]^T = \left[\frac{di_{dg}}{dt} \ \frac{di_{qg}}{dt} \right]^T.$$

In this work, the MLI is operating in active and reactive power control mode, and the output states are taken as

$$Y = [i_{dg} \ i_{qg}]^T. \tag{11}$$

V. ADOPTION OF SLIDING MODE CONTROL

The feedback linearization as discussed in the earlier section can only be effectively adopted if the exact model of the system is known. However, it is not an easy task to obtain all the parameters of the system. Moreover, as the MLI involves many switchings within a single cycle across different voltage sources, even the parameters are known, the accurate model with prevailing nonlinearities is difficult to obtain. Furthermore, as the system operating point and parameters are subjected to change in the due course of operation, the developed model cannot represent the system accurately in succeeding operations. To resolve this, an SMC [19], [20] technique is incorporated in the controller. In SMC, the discrete switching action is generated in such a way that the state direction of the system is brought back to sliding surface and traced up to the equilibrium point.

A. Constitution of Sliding Surface and Stability Criterion

The state vector, which is obtained in a linearization process, as in Section IV, will be transformed into a new state vector, and subsequently, the new control input, once the SMC is incorporated in the controller. The SMC can be viewed as a combination of equivalent control and a switching control, as represented in (12). The equivalent control can be adopted from linearization process as described in Section IV while the switching control is responsible for nullifying the errors resulting from parameter variations changes and operating point changes.

$$U(t) = U_{\text{eq}}(t) + U_{\text{sw}} = U_{\text{eq}}(t) + \rho \cdot \tanh(\sigma) \tag{12}$$

where ρ is a positive constant and σ is the sliding surface. For the satisfactory operation of the controller, it is necessary to define the sliding surface. Here, two sliding surfaces, namely, σ_1 and σ_2 are to be defined, since (11) has two output states i_{dg} and i_{qg}. For the second-order state variables, the sliding surface

$\sigma(t)$ can be defined as

$$\sigma(t) = \frac{d \ \text{er}(t)}{dt} + K_i \ \text{er}(t) \tag{13}$$

where K_i is the positive constant and er(t) is the error in the output. In this paper, by considering the relative degree for both i_{dg} and i_{qg} as 1, the error in DG current is chosen as the sliding surface. Hence, $\sigma_1 = \text{er}_1 = i_{dg} - i_{d\text{ref}}$ and $\sigma_2 = \text{er}_2 = i_{qg} - i_{q\text{ref}}$. The sliding surface matrix σ with σ_1 and σ_2 as elements can be defined as

$$\sigma = [\sigma_1 \ \sigma_2]. \tag{14}$$

For extract conditions on the SMC control law, which can run the state path to the equilibrium point, a Lyapunov approach is considered here. The Lyapunov function can be represented as

$$G = \frac{1}{2}\sigma^2. \tag{15}$$

Lyapunov stability criterion states that "if G is a positive definite function and its derivative, i.e., dG/dt is negative definite, then the system is asymptotically stable"

$$\text{i.e.,} \quad \frac{dG}{dt} = \sigma \dot{\sigma}^T < 0. \tag{16}$$

To satisfy the condition $\sigma \dot{\sigma}^T < 0$, $\dot{\sigma}$ can be considered as $\rho \tanh(\sigma)$

$$\dot{\sigma}_1 = -\rho_1 \cdot \tanh(\sigma_1) \text{ and } \dot{\sigma}_2 = -\rho_2 \cdot \tanh(\sigma_2). \tag{17}$$

Substituting (14) into (17)

$$\dot{\sigma}_1 = -\rho_1 \cdot \tanh(i_{dg} - i_{d\text{ref}}) \text{ and}$$
$$\dot{\sigma}_2 = -\rho_2 \cdot \tanh(i_{qg} - i_{q\text{ref}}). \tag{18}$$

With the obtained new dynamics using SMC, the state vector can be represented as

$$\lambda_1 = \begin{bmatrix} \lambda_{11} \\ \lambda_{12} \end{bmatrix} = \begin{bmatrix} -\rho_1 \cdot \tanh(i_{dg} - i_{d\text{ref}}) \\ -\rho_2 \cdot \tanh(i_{qg} - i_{q\text{ref}}) \end{bmatrix}. \tag{19}$$

$i_{d\text{ref}}$ and $i_{q\text{ref}}$ can be obtained from (3). If the parameter of the system changes, then change in the system matrix is ΔA, and the system can be represented as

$$\dot{X} = (A + \Delta A)X + B(U_{\text{eq}} + U_{\text{sw}}) \tag{20}$$

$$\dot{X} = AX + BU_{\text{eq}} + \Delta AX + B\rho \tanh(\sigma). \tag{21}$$

The parameter dependence part ΔAX will be compensated by switching part $B\rho \tanh(\sigma)$. Hence, the barrier condition for the selection of ρ is

$$B\rho > \Delta AX \text{ (or) } \rho > [B^{-1}\Delta AX]. \tag{22}$$

As aforesaid, ρ is a positive constant; however, to cancel out the errors resulting from parameter variations, operating point changes, and external disturbances, ρ should be large. However, large value of ρ will just convert the smooth transition action of tanh into hard switching function, sign which will result in chattering in the output. On contrary, very small value of ρ is not enough to cancel the parameter and operating point dependencies. Moreover, small ρ will result in sluggish response.

This article has been accepted for inclusion in a future issue of this journal. Content is final as presented, with the exception of pagination.

6   IEEE SYSTEMS JOURNAL

Parameter	Value
Grid Voltage, V_g	11 kV
Grid frequency, f	50 Hz
Filter inductance, L_f	8mH
Filter Resistance, R_f	0.2Ω
Voltages sources, V_0, V_k	1600V, 3200V
Switching frequency, f_s	5 kHz
Sample time, T_s	50μs
Base power	1 MVA
Short circuit MVA	1000 MVA
Sliding mode parameter ρ	2

Fig. 6. Harmonic spectrum of phase voltage of the RSC SSPS MLI for 11 levels.

Fig. 5. Phase voltage waveform of the RSC SSPS MLI for 11 levels.

Fig. 7. Performance comparison of SMC and PI for step increase in active and reactive powers references.

Fig. 8. Comparison between SMC and PI for step decrease in active and reactive powers.

Hence, in this paper, a sufficiently large value of ρ is selected so that the controller renders quick response while not entering the chattering zone.

VI. RESULTS AND VALIDATIONS

This section discusses the performance of the MLI with PI and SMC. Different simulation studies are discussed first; later, these obtained results are validated in real-time environment using an Opal-RT system.

A. Simulation Results

The RSC-SSPS-based grid-connected MLI system with PI controller as well as with SMC is developed, as shown in Figs. 3 and 4, using MATLAB/Simulink environment. The PI controller is designed as per the procedure outlined in Section IV and its gain parameters are tuned using integral time squared error criterion. The SMC is designed according to the procedure discussed in Section V. The parameters of the system considered are presented in Table III.

The PWM scheme is designed such that the RSC-SSPS-based MLI synthesizes 11 levels in its open-circuit output phase voltage, as depicted in Fig. 5, and its corresponding harmonic spectrum is shown in Fig. 6, which shows that the THD in voltage is 11.93%. The performance of the MLI with designed PI and SMC controllers is examined for set point power feedings to the grid under different operating conditions. For simplicity, the powers in Figs. 7–11 are represented in per unit with a base value of 1 MVA.

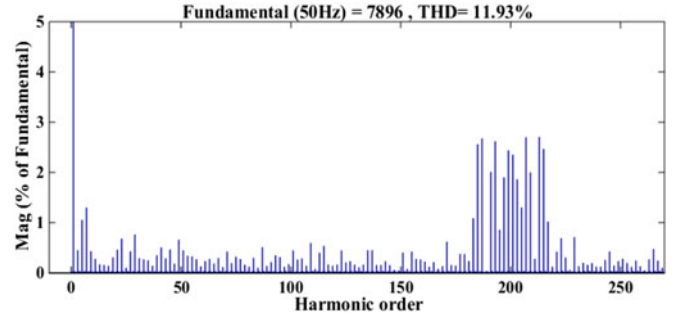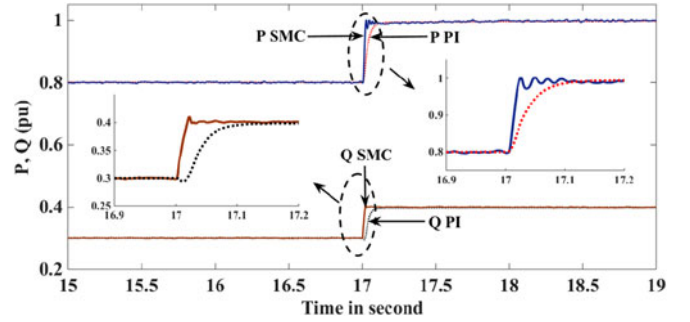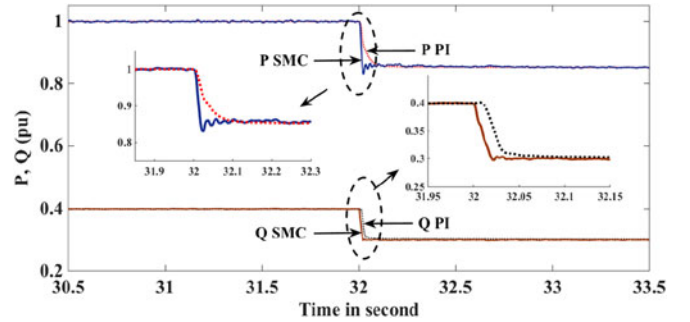*Case 1: Step change in active and reactive power references*

As shown in Fig. 7, active power reference (P_{ref}) is changed from 0.8 to 1 p.u. and reactive power reference (Q_{ref}) is changed from 0.3 to 0.4 p.u. at 17 s. It can be observed that SMC is able to track new P_{ref} within 3–4 cycles. The performance of PI is on par with SMC, except for the little delay in settling at the new reference powers. However, none of the controllers result in any appreciable over/undershoots, which can be seen in Fig. 7. Similarly, both SMC and PI exhibit very good performances for the decrease of reference powers, as shown in Fig. 8.

Case 2: Step change in reference reactive power with constant active power reference

In this case, Q_{ref} is changed from 0.4 to 0.3 p.u. while keeping P_{ref} as constant at 0.8 p.u. Performance of the MLI with SMC and PI controllers is shown in Fig. 9. It can be observed that the PI results a larger undershoot when compared with SMC, confirming the better decoupling control capability of SMC.

This article has been accepted for inclusion in a future issue of this journal. Content is final as presented, with the exception of pagination.

ESHWAR GOWD *et al.*: REAL-TIME VALIDATION OF A SLIDING MODE CONTROLLER FOR CLOSED-LOOP OPERATION OF REDUCED SWITCH 7
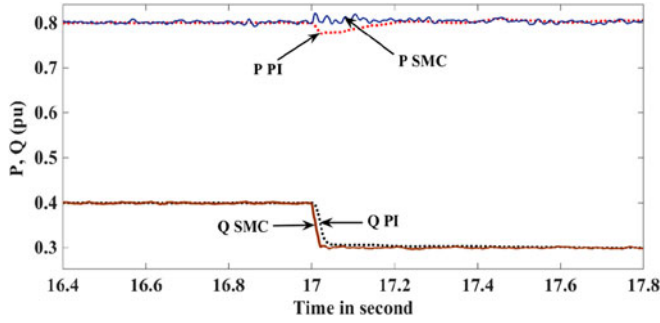

Fig. 9.   Performance of PI and SMC for a step change in reactive power and constant active power.
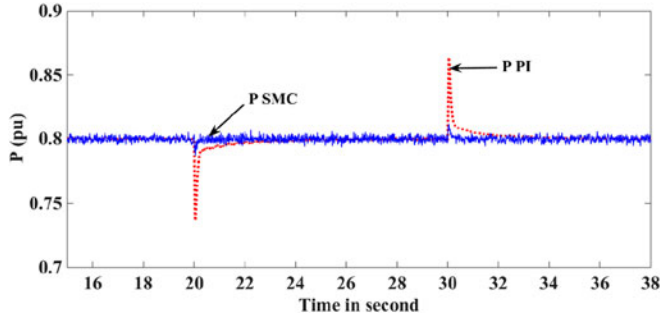
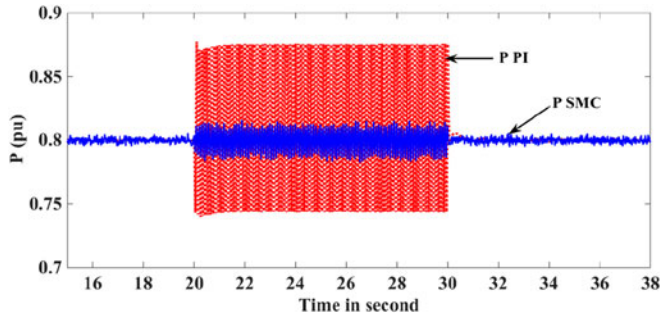Fig. 10.   Active power for step change in frequency under SMC and PI.

Fig. 11.   Active power for step change in frequency under SMC and PI.

Similar phenomenon can be observed for only change in real power reference while keeping the reactive power as constant.

Case 3: Change in grid frequency

This test is framed to examine the adaptability of gains of both the controllers. At first, the grid frequency is considered to be varied by 1 Hz at 20 s (i.e., from 50 to 51 Hz) and reaches 50 Hz at 30 s. For this step change in frequency, the performance of both the controllers is shown in Fig. 10. Even though both the controllers are driven by the same phase-locked loop, the SMC is able to adjust its gain very quickly and delivers extraordinary performance without any over/undershoots and with very small settling time, as shown in Fig. 10.

To validate the controllers further under varying grid frequencies, the grid frequency is subjected to continuous variation of 0.25 Hz magnitude from 20 to 30 s, to represent the modal frequency oscillations in the power system. The performance of the controllers is depicted in Fig. 11. Since the PI controller is a fixed gain controller, it is unable to adapt its gains and deliver highly oscillating performance, as shown in Fig. 11. However,
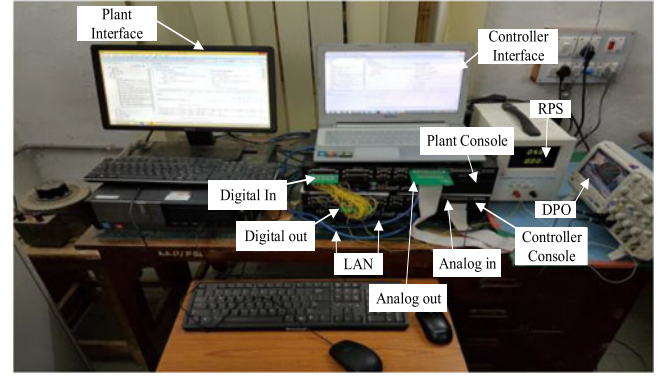

Fig. 12.   OPAL-RT real-time environmental setup.

the SMC delivers superior performance with very minimum oscillations when compared with the PI controller. This is due to the inherent nature of SMC, which is capable of adapting its gain according to the distance of the error from the defined error sliding surface.

Another important conclusion that can be drawn from this case is that with slight change in the frequency, be it a step change or continuous change, the PI controller results large overshoots/undershoots in output or results very high oscillatory performance. This nature of the performance of the PI controller may activate the over current protection gear in the system, hence completely disconnecting the MLI from the system; otherwise, the switches in the MLI will get damaged, which is undesirable. On the other hand, SMC delivers the required set-point powers without any deviations even under variations in the frequency; hence, the protection gear will remain inactive. Thereby, SMC eliminates the necessity of disconnection of the MLI by keeping the currents/powers well within the limits, hence contributing to the system stability under these operating disturbances.

Therefore, it can be concluded from the above-mentioned discussions that for all the test cases considered, SMC delivers either superior performance or its performance is on par with the PI controller. In no case, the performance of SMC is inferior to the PI controller. Moreover, SMC exhibits extraordinary performance under grid frequency variations while feeding of set-point real and reactive powers from the RSC-SSPS-based MLI.

B. Real-Time Validation With OPAL-RT

The OPAL-RT systems have proven record in validating the complex systems and their controls. Hence, this paper considered the same platform to validate the performance of the proposed RSC-SSPS-based MLI connected to the grid. This MLI is controlled either by SMC or PI controller. To verify the performance of the proposed three-phase RSC-SSPS-based MLI in real-time environment, two OP4500 modules of OPAL-RT are integrated, as shown in Fig. 12. To analyze the complete grid interfacing system, one of the modules works as a plant, that is, grid-connected SSPS MLI, whereas the other module works as a controller, that is, SMC/PI-based PWM generator. The plant
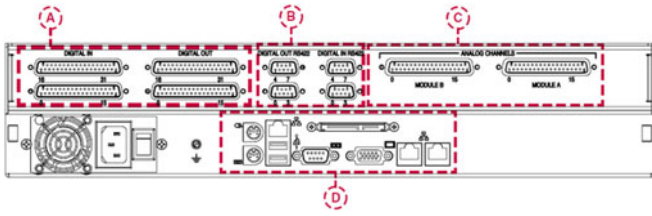
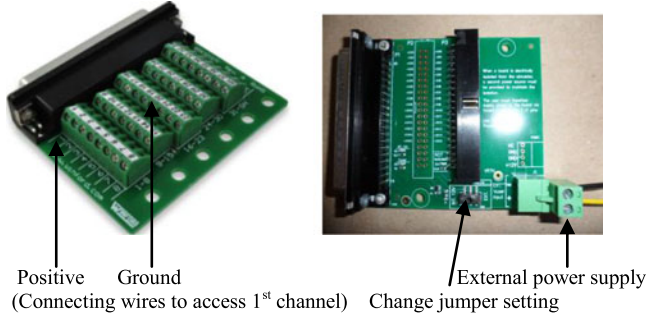Fig. 13.   View of rear interface OP4500 [22].

Positive   Ground
(Connecting wires to access 1st channel)   Change jumper setting   External power supply

Fig. 14.   DB 37 screw terminals [22].

(a)   (b)

Fig. 15.   Powers feedings of the MLI to the grid for step increase in reference with (a) PI controller and (b) SMC (X-axis: 100 ms/div, Y-axis: 0.2 p.u./div).

(a)   (b)

Fig. 16.   Powers feedings of the MLI to the grid for step decrease in reference with (a) PI controller and (b) SMC (X-axis: 100 ms/div, Y-axis: 0.2 p.u./div).

(a)   (b)

Fig. 17.   Performance of the MLI for decoupling control of real and reactive powers feedings with (a) PI controller and (b) SMC (X-axis: 200 ms/div, Y-axis: 0.2 p.u./div).

(a)   (b)

Fig. 18. P_{grid} for step changes in grid frequency with (a) PI controller and (b) SMC (X-axis: 2 s/div, Y-axis: 0.2 p.u./div).

system along with its interface generates analog signals according to the operating conditions and disturbances, which will be acquired by a controller through a communication channel. The controller system generates necessary control actions according to the selected control scheme. The controller communicates the pulses to the plant in the form of digital signals. In order to validate the proposed closed-loop grid-connected MLI-based system in real-time using Opal-RT systems, the sampling time is taken as 50 μs, which gives the sampling frequency of 20 kHz. With this selection of sample time, the overrun errors are made zero, so that the real-time implementation will be more accurate. The rear view of the OPAL-RT module is shown in Fig. 13 with the typical access points for the digital input/output port (block A), analog input/output port (block C), differential input/output port (block B), and standard computer connection port (block D).

The connector DB37, which is shown in Fig. 14, is useful for the digital inputs/outputs and analog inputs/outputs of A and C blocks, respectively. As shown in Fig. 14, each DB37 connector is used to access 16 channels of the associated I/Os (either analog or digital). With these interfacings and involved interactions between two OP4500 modules, an hardware-in-loop (HIL) system of the proposed RSC-SSPS-based MLI is realized.

The responses for the closed-loop control system with SMC and PI control schemes are recorded by using a digital storage oscilloscope. The performance comparison of the proposed three-phase RSC-SSPS-based MLI in real-time environment is shown in Figs. 15–19, respectively, for simulation responses shown in Figs. 7–11. As inferred in simulation results, except for the slight delay in PI controller settling, both the PI and SMC perform satisfactorily for both increase and decrease of power references, which can be seen in Figs. 15 and 16.

The real-time validation of decoupling capability of SMC between real and reactive powers, as compared to the PI controller, is shown in Fig. 17. In this case study, only reactive power reference is changed while keeping the real power
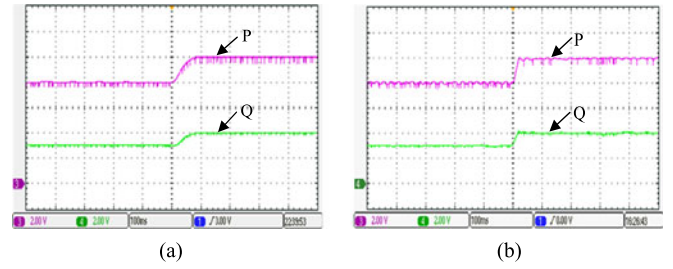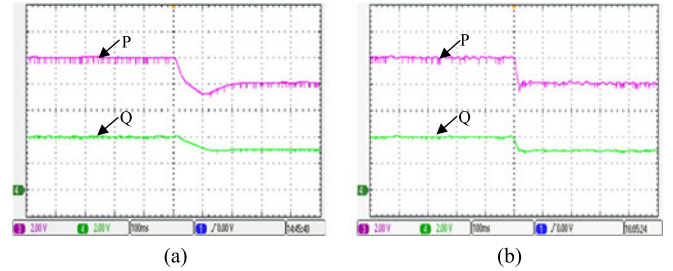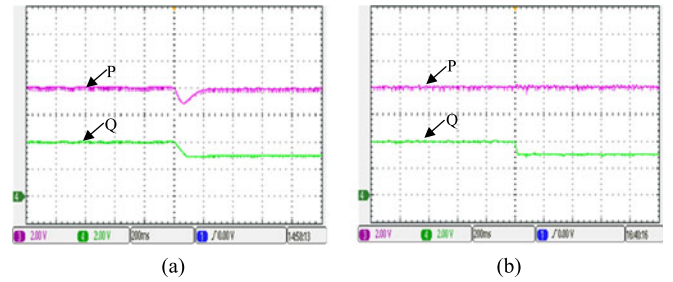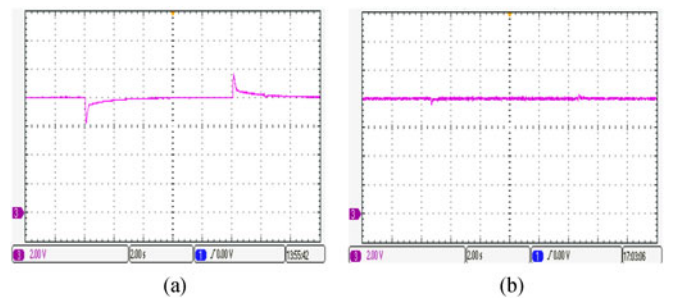
reference as constant. As shown in Fig. 17(a), though the real power feeding is maintained at the reference value, it experiences transients with the only change in reactive power reference, if it is controlled by a PI controller. Contrarily, the real power feeding is unaffected by the disturbance in the reactive power feeding when the MLI is controlled by SMC, as shown in Fig. 17(b).

The performance of the system with both the control schemes under grid frequency variations is shown in Figs. 18 and 19. For the change in grid frequency of 1 Hz, the PI controller deliv-
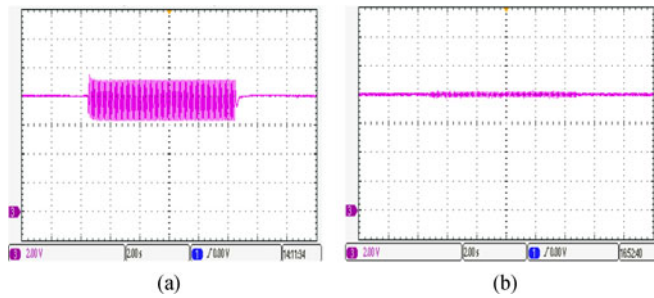
Fig. 19. Real power feeding by the RSC-SSPS-based MLI to the grid for frequency oscillations with (a) PI controller and (b) SMC (*X*-axis: 2 s/div, *Y*-axis 0.2 p.u./div).

ers power with overshoots/undershoots, as shown in Fig. 18(a), while the SMC is able to adopt its gain and ensure smooth power delivery to the grid, as shown in Fig. 18(b). For a continuous change in grid frequency, which represents modal frequency oscillations, the PI delivers quite oscillatory performance with large amount of power deviations, as shown in Fig. 19(a). It can trigger the overcurrent protection of the converter. Hence, the response of the PI controller, which cannot adapt its gains, is a potential candidate to create instability in the system by disconnecting the converter, which supplies power to the grid. On contrary, the system with SMC delivers almost a smooth power, as shown in Fig. 19(b), thereby ensuring that the converter remains connected to the grid during the disturbances. Therefore, it can be understood that the RSC-SSPS-based MLI with SMC can operate more stably and can override the disturbances. Hence, confirming all the simulation responses discussed in Section VI-A.

VII. Conclusion

Sliding mode based nonlinear controller for the closed-loop operation of the three-phase MLI with reduced number of switches is developed in this paper. Through series/parallel switchings, this RSC-SSPS MLI topology utilizes the available dc sources more effectively when compared with CHB topologies. It is concluded that the MLI with PI experiences large overshoots/undershoots in power delivery under grid frequency variations, thereby activating the protection system of the converter, which disconnects the MLI from the rest of the system. On the other hand, with negligible overshoots/undershoots, the MLI with SMC can override the frequency disturbances and can retain the MLI connected with the grid even under disturbances, thereby supporting system to regain its stability. The conclusions drawn from simulations are validated in real-time environment using Opal-RT systems.

References

[1] M. F. Kangarlu and E. Babaei, "Cross-switched multilevel inverter: An innovative topology," *IET Power Electron.*, vol. 6, no. 4, pp. 642–651, 2013.

[2] Z. Lim, A. I. Maswood, and G. H. P. Ooi, "Modular-cell inverter employing reduced flying capacitors with hybrid phase-shifted carrier phase-disposition PWM," *IEEE Trans. Ind. Electron.*, vol. 62, no. 7, pp. 4086–4095, Jul. 2015.

[3] H. Belkame, S. Mekhilef, A. Masaoud, and M. A. Naeim, "Novel three-phase asymmetrical cascaded multilevel voltage source inverter," *IET Power Electron.*, vol. 6, no. 8, pp. 1696–1706, 2013.

[4] A. Masaoud, H. W. Ping, S. Mekhilef, and A. S. Taallah, "New three-phase multilevel inverter with reduced number of power electronic components," *IEEE Trans. Power Electron.*, vol. 29, no. 11, pp. 6018–6029, Nov. 2014.

[5] G.-J. Su, "Multilevel dc-link inverter," *IEEE Trans. Ind. Electron.*, vol. 41, no. 3, pp. 848–854, May/Jun. 2005.

[6] E. Najafi, A. Halim, and M. Yatim, "Design and Implementation of a new multilevel inverter topology," *IEEE Trans. Ind. Electron.*, vol. 59, no. 11, pp. 4148–4154, Nov. 2012.

[7] A. Salem, E. M. Ahmed, M. Orabi, and M. Ahme, "New three-phase symmetrical multilevel voltage source inverter," *IEEE J. Emerging Sel. Topics Circuits Syst.*, vol. 5, no. 3, pp. 430–441, Sep. 2015.

[8] K. K. Gupta, A. Ranjan, P. Bhavnagar, L. K. Sahu, and S. Jain, "Multilevel inverter topologies with reduced device count: A review," *IEEE Trans. Power Electron.*, vol. 31, no. 1, pp. 135–151, Jan. 2016.

[9] F. L. Luo and H. Ye, "Laddered multilevel dc/ac inverters used in solar panel energy systems," *IET Power Electron.*, vol. 6, no. 9, pp. 1769–1777, 2013.

[10] E. Zamiri, N. Vosoughi, S. Hossein, R. Barzegarkhoo, and M. Sabahi, "A new cascaded switched-capacitor multilevel inverter based on improved series–parallel conversion with less number of components," *IEEE Trans. Ind. Electron.*, vol. 63, no. 6, pp. 3582–3594, Jun. 2016.

[11] Y. Hinago and H. Koizumi, "A switched-capacitor inverter using series/parallel conversion with inductive load," *IEEE Trans. Ind. Electron.*, vol. 59, no. 2, pp. 878–886, Feb. 2012.

[12] J.-S. Lai and F. Z. Peng, "Multilevel converters-a new breed of power converters," *IEEE Trans. Ind. Appl.*, vol. 32, no. 3, pp. 509–517, May/Jun. 1996.

[13] Y. Hinago and H. Koizumi, "A single-phase multilevel inverter using switched series/parallel dc voltage sources," *IEEE Trans. Ind. Electron.*, vol. 57, no. 8, pp. 2643–2650, Aug. 2010.

[14] B. Xiao, L. Hang, J. Mei, C. Riley, L. M. Tolbert, and B. Ozpineci, "Modular cascaded H-bridge multilevel PV inverter with distributed MPPT for grid-connected applications," *IEEE Trans. Ind. Appl.*, vol. 51, no. 2, pp. 1722–1731, Mar./Apr. 2015.

[15] Y. Shi, R. Li, Y. Xue, and H. Li, "High-frequency-link-based grid-tied PV system with small dc-link capacitor and low-frequency ripple-free maximum power point tracking," *IEEE Trans. Power Electron.*, vol. 31, no. 1, pp. 328–339, Jan. 2016.

[16] E. Villanueva, P. Correa, J. Rodríguez, and M. Pacas, "Control of a single-phase cascaded H-bridge multilevel inverter for grid-connected photovoltaic systems," *IEEE Trans. Ind. Electron.*, vol. 56, no. 11, pp. 4399–4406, Nov. 2009.

[17] L. He, K. Zhang, J. Xiong, and S. Fan, "A repetitive control scheme for harmonic suppression of circulating current in modular multilevel converters," *IEEE Trans. Power Electron.*, vol. 30, no. 1, pp. 471–481, Jan. 2015.

[18] L. Ben-Brahim, A. Gastli, M. Trabelsi, K. A. Ghazi, M. Houchati, and H. Abu-Rub, "Modular multilevel converter circulating current reduction using model predictive control," *IEEE Trans. Ind. Electron.*, vol. 63, no. 6, pp. 3857–3866, Jun. 2016.

[19] A. Moharana and P. K. Das, "Input-output linearization and robust sliding-mode controller for the VSC-HVDC transmission link," *IEEE Trans. Power. Del.*, vol. 25, no. 3, pp. 1952–1961, Jul. 2010.

[20] S. Mishra and P. C. Sekhar, "Sliding mode based feedback linearizing controller for a PV system to improve the performance under grid frequency variation," in *Proc. IEEE Int. Conf. Energy, Autom. Signal*, Dec. 2011, pp. 1–7.

[21] F. Sebaaly, H. Vahedi, H. Y. Kanaan, N. Moubayed, and K. Al-Haddad, "Design and implementation of space vector modulation-based sliding mode control for grid-connected 3L-NPC inverter," *IEEE Trans. Ind. Electron.*, vol. 63, no. 12, pp. 7854–7863, Dec. 2016.

[22] "Op4500 RT-Lab-RCP/HIL system user guide." [Online]. Available: http://www.opal-rt.com/wp-content/themes/enfold-opal/pdf/L00161_0331.pdf

G. Eshwar Gowd received the B.Tech. and M.Tech. degrees from Jawaharlal Nehru Technological University, Anantapur, India. Currently, he is working toward the Ph.D. degree with the National Institute of Technology Warangal, Warangal, India.

His current research interests include multilevel inverters design, power electronics control, and renewable energy systems.

P. C. Sekhar received the B.Tech. degree in electrical and electronics engineering from Jawaharlal Nehru Technological University, Hyderabad, India, the M.Tech. degree in electrical engineering from the National Institute of Technology Rourkela, Rourkela, India, and the Ph.D. degree in electrical engineering from the Indian Institute of Technology Delhi, New Delhi, India.

He was an Assistant Professor with the National Institute of Technology Warangal, from 2014 to 2017, and is currently an Assistant Professor with the School of Electrical Sciences, Indian Institute of Technology Bhubaneswar, Bhubaneswar, India. He was a Transnational Access Researcher with The National Smart Grid Laboratory, Trondheim, Norway, in 2017 under H2020 Programme. His research interests include integration and control of renewable energy systems, design and development of smart controllers for microgrid/smart grid systems, control of active distribution systems, and power electronics applications in power systems.

Dr. Sekhar was a recipient of the Young Engineer Award from Institution of Engineers (India), in 2017; the Early Career Research Award (Young Scientist) from the Department of Science and Technology, Government of India, in 2016; the Innovative Ph.D. Thesis Award (Best Thesis) from the Indian National Academy of Engineering, in 2015; Madusudan Memorial Medal from The Institution of Engineers (India) in 2009; and the POSOCO Power Systems Award from Power Grid Corporation of India, in 2013. He has been selected for Indo-US Postdoctoral Fellowship and SERB-Overseas Postdoctoral Fellowship.

Dharmavarapu Sreenivasarao born in Andhra Pradesh, India. He received the M.Tech. and Ph.D. degrees in electrical engineering from the Indian Institute of Technology Roorkee, Roorkee, India, in 2008 and 2014, respectively.

He is currently an Assistant Professor with the National Institute of Technology Warangal, Warangal, India. His research interests include new converter topologies, modulation techniques for multilevel inverters, electric vehicles, power quality, and adjustable-speed drives.